Automated building energy modeling for existing buildings using computer vision

Ipek Gursel Dino[1 2, *], Esat Kalfaoglu[1], Alp Eren Sarı[1], Sahin Akin[1], Orcun Koral Iseri[1], A. Aydın Alatan[1], Sinan Kalkan[1], Bilge Erdogan[2]

[1] Center for Image Analysis (OGAM), Middle East Technical University, Turkey
[2] Department of Architecture, Middle East Technical University, Turkey
[2] Heriot-Watt University, United Kingdom
*email: ipekg@metu.edu.tr

Abstract

Improving the energy efficiency of existing buildings requires energy models that accurately represent the building and quantify various performance measures. Manual energy modeling has been proven to be inefficient, labor-intensive and error-prone. Therefore, the automation of energy modelling is critical. Existing approaches for 3D geometry extraction using 3D laser scanning are promising, but their high cost and high level of operational expertise prevent their widespread use. Computer vision methods, particularly 3D reconstruction can effectively support the creation of 3D building models. An additional component of energy models is the building envelope's thermal characteristics. IR thermography can be used to determine the thermal transmittance of the external walls with data collection in both visible and thermal bands. This paper presents a method for the semi-automated energy modeling of existing buildings. A conventional structure-from-motion (SfM) pipeline is utilized, which consists of several algorithms that compute a 3D point cloud from the images of the room to be modelled. The system matches the image points of the same scene points on different views by using Scale Invariant Feature Transform (SIFT) features and L2 Cascade Hashing with precomputed hashed regions methods to match the calculated features and perform 3D reconstruction using incremental SfM. Following, the two cameras are calibrated, after which each point in the point cloud is matched with the corresponding temperature measured by a thermal camera after using the intrinsic and extrinsic parameters of the optical and thermographic cameras. A planar surface representing each surface is calculated, and the elimination of objects other that building surfaces is performed by a Random Sample Consensus (RANSAC) algorithm. Finally, thermal transmittance values of the outer walls are calculated using the measured surface temperatures. The results are validated in two steps. The first step calculates the difference between the geometry of the 3D ground truth model of the actual room and the generated 3d model. The second step is a comparative analysis between the calculated energy use of two energy models (using Energyplus) constructed with different methods: the manual method (using as-built drawings and theoretical thermal transmittance values) and the proposed method. The difference between the simulation results of these two models are finally comparatively analyzed. The initial results are expected to be indicative of the benefits of using semi-automated methods of energy model construction for existing buildings.

Keywords: 3D reconstruction, thermography, building energy modeling, building energy performance

1. Introduction

Improving the energy efficiency of existing buildings call for approaches that precisely quantify energy use through energy modeling and simulation, as a response to the increasing complexity of buildings and systems. Energy simulation has the potential to reduce buildings' environmental impact, improve occupant comfort and indoor environmental quality and facilitate innovation in AEC (Hensen & Lamberts, 2011). For existing buildings, energy simulations have the potential to complement real

monitored building data for operational optimization or retrofit. While a building can only react to actual contextual conditions such as local weather, occupancy, operational patterns, a simulation-based virtual model can move back in time to analyze the building's past behavior to calibrate the program for improved predictive potency, or move forward in time to predict the building's response to alternative control scenarios (Mahdavi, 2001). Dynamic energy simulation tools adopt a forward-modeling approach that begins with a description of the building and components, providing a physical description of the building (design geometry, construction data, thermal zones, internal heat gain, infiltration and usage profiles), its systems (system types and sizes, control schedules, outdoor air requirements) and components (HVAC components) (Wang, Yan, & Xiao, 2012). Amongst these, the former is the most fundamental category that the other categories are based upon. Therefore, a correct description of the building is critical for the reliability of simulation-based performance assessment.

Despite the key role of simulations in performance assessment, the difficulties in the construction of energy models has been a major obstacle against their widespread use. Manual modelling efforts are based on building documentation (i.e. drawings, specifications, schedules) and walk-through audits. However, this process is labor-intensive and might result in disparities between the building and the model. This is due to (1) buildings undergoing undocumented major changes, (2) the degradation of materials over time, and (3) the difficulties in capturing internal load patterns and dynamic components for extended periods of time. ICT techniques can help automate energy modelling. 3D laser scanning is a promising technology for 3D geometry extraction for planning retrofit, spatial planning, resource and construction progress tracking (Akinci et al., 2006; Bosché & Guenet, 2014a, 2014b; Bosché, Guillemet, Turkan, Haas, & Haas, 2013; Dimitrov & Golparvar-Fard, 2014; Mahdjoubi, Moobela, & Laing, 2013; Valero, Adan, & Cerrada, 2012). However, its high cost, high level of operational expertise and complexity prevent its widespread use.

An effective and inexpensive alternative is 3D reconstruction. Computer vision research has been studying 3D reconstruction in any scale by utilizing the multiple photos taken by any camera at any time. Any 3D structure generation pipeline has a number of stages including calibration, pose estimation, triangulation and parameter optimization of the 3D structure (Sweeney, 2015). While 3D reconstruction from a collection of images has been previously addressed widely, many research problems remain unsolved in each stage of a generic pipeline from an energy modeling viewpoint. The latter method, thermal imaging, is the act of recording temperature variations of a surface in visible images. Thermal imaging offers a non-destructive and rapid way to calculate material thermal properties (U-value) from surface temperatures. When 2D images and thermal images are captured and merged, a 3D building model with material properties can be generated. A novel approach needs to be developed for the registration of thermal (low spatial resolution) images captured by thermographic cameras on the initial 3D models. Moreover, the approach should address several requirements regarding energy modeling. The first requirements is the generation of the 3D model of the building or the room. Energy models represent building surfaces as planar surfaces without thickness (thickness is typically added elsewhere by material association) to calculate heat transfer. For each room, a seamless volume bounded by a minimum number of surfaces is needed to be defined to avoid unnecessary computational cost. Therefore, the 3D point cloud captured through 3D reconstruction needs to be processed to generate a polygon model. Moreover, during 3D reconstruction, a complete optical view of surfaces that allows the construction of a complete wall surface might not be available due to occlusion or clutter. The second requirement is the calculation of thermal resistance data of external wall surfaces. Material thermal properties is a determinant factor in building energy use. Thermal imaging can help calculate thermal resistance values of building constructions from surface temperatures. An existing method that calculates R-values at the level of 3D points is used in this research. Final, data integration with energy modeling tools is needed to transfer the captured data an energy modeling tool, EnergyPlus.

2. Material and methods

This paper proposes a method for the semi-automated energy modeling of existing buildings using 3D reconstruction. Specifically, a pipeline that merges digital 2D optical images and thermal images of a room into a single 3D building model with surface thermal resistance values is developed. The pipeline uses visual band images registered with corresponding thermal images as input data. The main steps of

the pipeline are the calibration of the imaging system, 3D model generation, fusion and thermal resistance calculation (Figure 1). Details for each step is provided in the following subsections. We used two types of images together, which are visual band and thermal images. Visual band images are utilized for 3D model generation and thermal images are utilized for thermal resistance calculation.

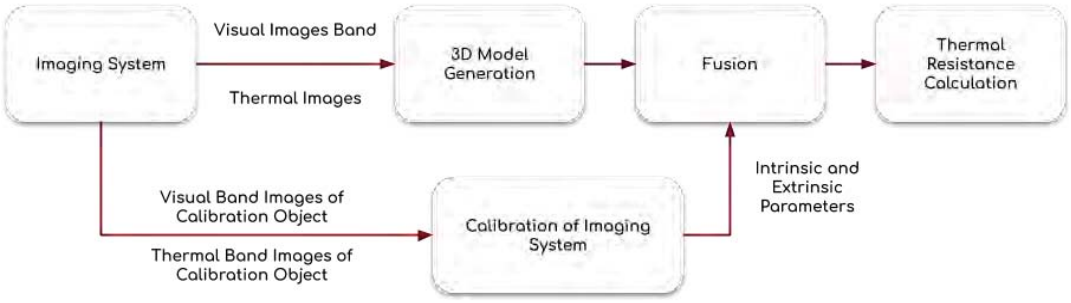

Figure 1. The proposed pipeline

2.1 The Calibration of the Imaging System

Physical properties of a camera are defined by its intrinsic parameters, that are focal lengths and optical centers. Therefore, it is essential to first calculate the intrinsic parameters of the visual band and thermal cameras while generating a 3D model. The process of computing the intrinsic and extrinsic (rotation and translation) parameters of a camera at the same time is known as camera calibration in computer vision. We calibrated both our visual band and thermal cameras using MATLAB's camera calibration toolbox. We also calculate the relative pose (i.e. rotation matrix and translation vector) between coordinate systems of the visual band and thermal cameras to map pixels between these cameras.

a. Visual Band Calibration: We manufactured a checkerboard calibration object using a piece of cardboard, whose images were taken by the visual band camera (Figure 2 - Left). We calculated the intrinsic and extrinsic parameters of the visual band camera with 20 pictures of the calibration object captured by the camera.
b. Thermal Calibration: The same calibration is used for the calibration of the thermal camera since the checkerboard pattern is observable in the thermal image, (Figure 2 - Right). We similarly calculate the intrinsic and extrinsic parameters of the thermal camera using 20 images of the calibration object captured by the thermal camera.
c. Pose estimation between the two cameras: The intrinsic parameters (translation and rotation) were obtained with respect to the same calibration object for both visual band and thermal cameras. We exploit this fact to calculate the relative translation and rotation between the two cameras. It should be noted that since both cameras capture images of the calibration object at the same time, the calculation of translation and rotation between the two cameras was possible due to the fact that two sensors are mounted on the same body. We calculate the rotation matrices and translation vectors between each image in the visual band and thermal cameras, and finally take the average of the estimated data to find a single robust rotation matrix and translation vector.

Figure 2. The checkerboards used for calibration

2.2 3D Model Generation

For generating an accurate 3D model of the room, we mainly rely on a widely-used technique in computer vision, namely, Structure from Motion (SfM). In SfM, a set of images of an environment are used to obtain 3D information about the environment. These images are assumed to be captured at different positions (and possibly with different cameras) and to contain overlapping views of the environment. From the overlapping views, or more technically, the visual information that correspond to the same 3D entities in the environment, the positions of the cameras and the 3D coordinates of the pixels can be identified. For 3D model generation, we adapted OpenMVG's tools to form a pipeline, which is composed of visual information (feature) description, visual feature matching, SfM, multiview stereo and enhancement through interaction (Moulon, Monasse, Perrot, & Marlet, 2017).

a. Visual Feature Description: Not every pixel in an image carries visually meaningful information. To find those useful pixels (also called keypoints) as well as representing information at and around those keypoints, we use the Scale-Invariant Feature Transform (SIFT) method (Lowe, 2004). SIFT finds keypoints by looking at intensity changes in an image at multiple scales. If there is a consistent change at a pixel at different scales, then that pixel is assumed to carry useful information. For representing such a keypoint, SIFT calculates a summary of how the intensity changes around the keypoint in the form of a 128-dimensional vector.
b. Visual Feature Matching: The computed feature vectors are first matched using the algorithm, which results in a set of potential matches between features in different views (Cheng, Leng, Wu, Cui, & Lu, 2014). Following, a geometric filtering operation is employed to choose the geometrically meaningful matches using AC-RANSAC (A Contrario RANdom SAmple Consensus) (Moulon et al., 2012).
c. Structure from Motion (SfM): For SfM, we use the method proposed by Moulon et al. (2012) due to its robustness and adaptive capacity. The method constructs an initial 3D model using the best matching two images and continues reconstruction by adding the remaining images repeatedly.

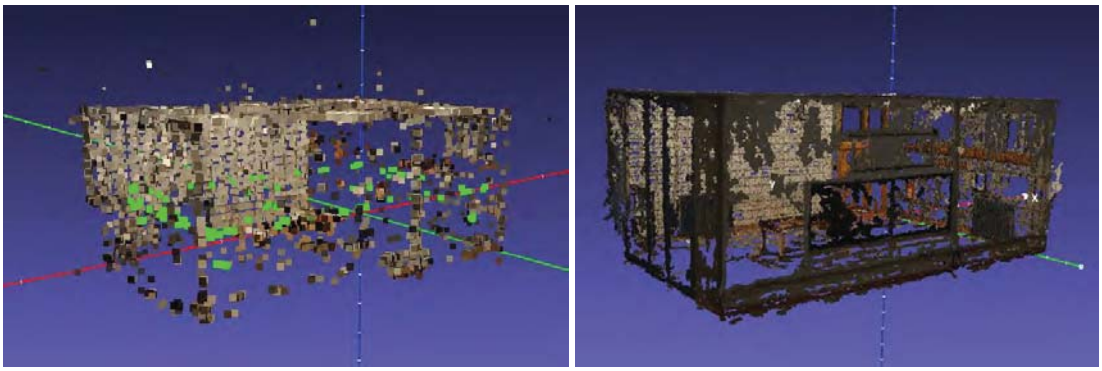

Figure 3. The sparse 3D model (left) and the densified 3D point cloud

d. Densification using Multi-view Stereo (MVS): Since a dense 3D point cloud is needed for 3D reconstruction, it is essential to densify the sparse 3D point cloud computed by SfM. For densification, we employed an algorithm for Multiview stereopsis developed by Furukawa et al. (2010), which densifies a given 3D point cloud by interpolation. The sparse and dense point clouds can be seen in Figure 3.
e. Enhancement through Interaction: In the previous step, a 3D model of the environment has been obtained. To finalize the model for the following steps, several post-processing phases were followed:

i. Adjusting the Scale and Pose of the 3D Model: We first select some points from the captured visual band images (Figure 4) and find their actual 3D coordinates by measuring the physical distances between them. Following, we compute a similarity transformation with non-linear optimization that provides the lowest mean squares error. This similarity transformation is applied onto the reconstructed 3D point cloud to correct the scale, orientation and translation of the 3D point cloud. However, this process can introduce some degree of imprecision, since might not be possible to match the exact pixel/location in the calculated 3D points.

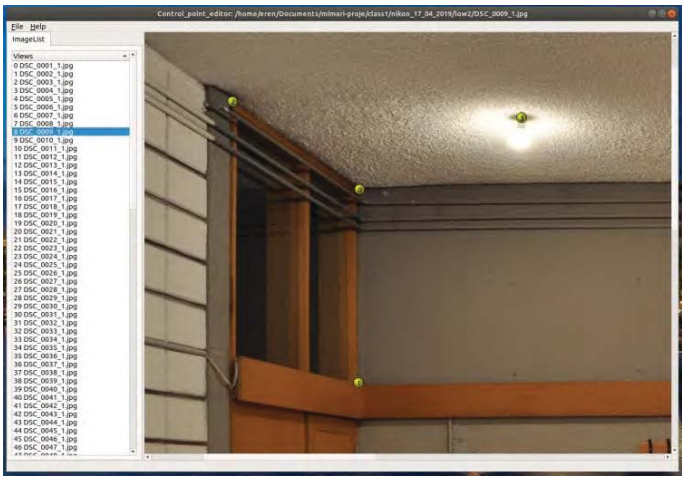

Figure 4: Point selection from captured images

ii. *Calculating the surfaces in the model:* The equations of a plane for each surface (walls, floor and ceiling) are computed for the points that lie within a rectangular shape that is manually marked by the user on the images (Figure 5). Plane estimation from a set of 3D points is performed using least-squares estimation. Specifically, the Singular Value Decomposition method is used, where the last column of the V matrix represents the plane equation. After plane fitting, the corners of the room are calculated by intersecting the corresponding three planes for each corner (Eq 1),

$$\boldsymbol{X}_{Nx4} = \boldsymbol{U}_{NxN}\boldsymbol{\Sigma}_{Nx4}\boldsymbol{V}^{T}_{4x4}, \qquad \text{Eq. 1}$$

where $\boldsymbol{X}$ is a Nx4 matrix whose first 3 rows contain the 3D points in the selected rectangle and the fourth row contains a vector of 1's with dimensions Nx1, the matrices $\boldsymbol{U}$, $\boldsymbol{\Sigma}$, $\boldsymbol{V}$ are the singular value decomposition (SVD) of the $\boldsymbol{X}$ matrix. The last column of $\boldsymbol{V}$ is the plane coefficient, which provides the best fit to the selected 3D points.

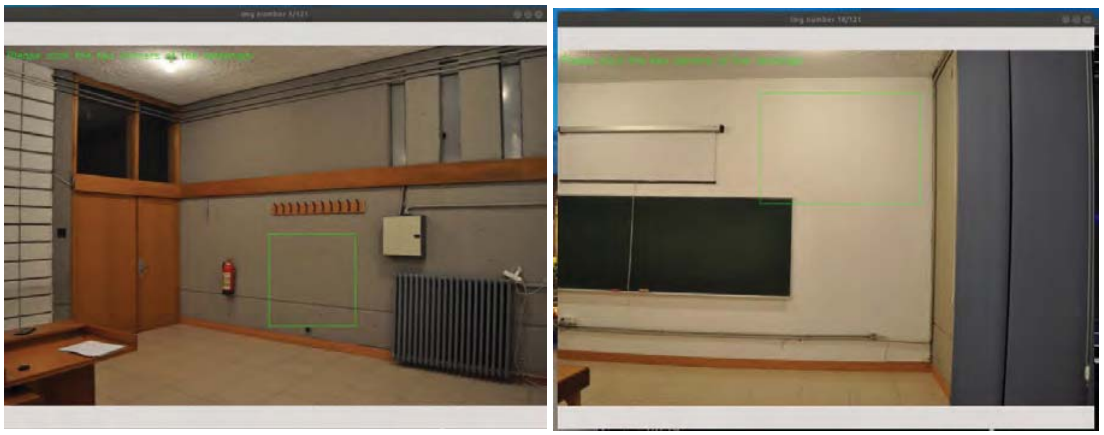

Figure 5. Point selection from the east (left) and south (right) walls

iii. *Window and Door Detection:* The corners of the windows and the doors are selected by the users. An example of selecting the window corners can be seen in Figure 6-C. After this step, the corresponding 3D points for each corner point are calculated by projecting the 3D point cloud onto the corresponding image and searching for the best match for the points selected and they are projected onto the previously calculated planes.

Figure 6. A. Identification of the wall planes by selecting certain areas on the surfaces, B. Selection of the surface photos for surface creation, C. Identification of the window surfaces by selecting a certain area on the desired window. D. Selection of the desired window photos for window creation

2.3. Fusion with Thermal Data

During this step, the captured thermal images are mapped to the 3D model to calculate the thermal resistance values for the external walls. To this end, the (intrinsic) parameters of visual band (RGB) and thermal cameras and the relative 3D rotation and 3D translation between them are used. The following steps were followed.

- Calculating the rotation and translation of each visual band image by multiplying each RGB camera's projection with the inverse of the visual band camera's intrinsic matrix.

$$P_{RGB} = K_{RGB}[R_{RGB}t_{RGB}]$$
$$[R_{RGB}t_{RGB}] = K^{-1}P_{RGB} \quad \text{Eq. 2}$$

where P_{RGB} is the projection matrix of the RGB camera, K_{RGB} is the intrinsic matrix of the RGB camera, R_{RGB} is the rotation matrix of the RGB camera and t_{RGB} is the translation vector of the RGB camera.

- Multiplying the rotation matrices calculated at the previous step with the rotation matrix that corresponds to the rotation between RGB and thermal cameras, and adding the translation vector between RGB and thermal cameras to each RGB camera's translation. The rotation and the translation values of each thermal camera are calculated as follows:

$$R_{thermal} = R_{relative}R_{RGB}^{T}$$
$$t_{thermal} = R_{RGB}^{T}t_{RGB} + t_{relative} \quad \text{Eq. 3}$$
$$P_{thermal} = K_{thermal}[R_{thermal}t_{thermal}]$$

  where Rthermal is the rotation matrix of the thermal camera, Rrelative is the rotation matrix of the rotation difference between the RGB and the thermal cameras, tthermal is the translation vector of the thermal camera, trelative is the translation vector of the translation difference between the RGB and the thermal camera, Pthermal is the projection matrix and Kthermal is the intrinsic matrix of the thermal camera.

- Stacking the calculated rotation matrices and translation vectors into matrices, and multiplying these matrices with the intrinsic matrix of the thermal camera.
- Each 3D point of the point cloud is projected onto thermal images' planes using the previously calculated projection matrices. Afterwards, the depth and the projected coordinates are checked. If the depth and the projected coordinates are both positive and within the image's coordinates, they are accepted as point correspondences and the RGB color of the thermal image point is assigned to its corresponding 3D point (Figure 7).

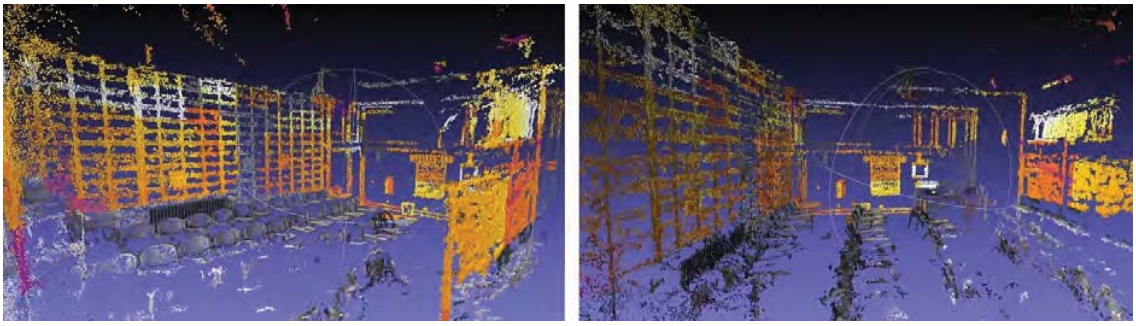

Figure 7. Juxtaposition of the thermal images on the point cloud.

2.4. Calculation of Thermal Resistance

Thermal resistance values of the external walls are calculated using the method proposed by Ham et. al (Ham & Golparvar-Fard, 2013). For each wall, the mean surface temperature is first calculated using the thermal point cloud and calculated planes and these mean temperature values are used to calculate the thermal resistance values. The equation for thermal resistance calculation is given by Ham et al. as:

$$R = \frac{\left|T_{inside,air} - T_{outside,air}\right|}{\alpha_{con} \times \left|T_{inside,air} - T_{inside,wall}\right| + \epsilon \times \sigma \times \left|T_{inside,wall}^{4} - T_{inside,reflected}^{4}\right|}, \quad \text{Eq. 4}$$

where α_{con} is the convective heat transfer coefficient, ε is the thermal emissivity, and σ is the Stefan-Boltzmann coefficient. Following this equation, room mean air temperature is measured using a thermometer and the reflected temperature is measured by capturing an image of a crumpled aluminum coil with the thermal camera and taking the mean value of the temperatures of the aluminum coil.

Together with the described pipeline, a graphical user interface (GUI) was designed to allow the users select the optical and thermographic images for 3D reconstruction, manually mark the surfaces of walls on optical images for plane construction and mark the boundaries of windows and doors to define these elements in the model. Once the previous steps are completed, the generated data (corner points of planes, R values, window and door points) is written in XML format with an XML schema developed by us. This file is read by a parser to construct a surface model for 3D model validation (section 3.1), and by OpenStudio SDK, an open-source framework that provides access to EnergyPlus object attributes (Weaver et al., 2019) for building energy modeling (section 3.2).

3. Results

The developed method was implemented in a classroom with an area of 46.48 m^2 in an educational building. Both electrooptic images and thermal images are captured using a FLIR E60 camera. FLIR 60 has a thermal sensitivity of <0.05°C, with an 800-pixel resolution for infrared images (320 x 240) and 3.1-megapixel resolution digital camera. The images were captured, and measurements were taken on 24 December 2018 at 6:00AM, to achieve a quasi-steady-state condition of heat transfer. The captured images, both electrooptic and thermal, were processed through the proposed pipeline. During this process, only the walls, ceiling and floor are used for model construction. The results of two comparative analyses are presented in the following sections.

3.1 3D model validation

This section presents the results of the comparative analysis between the 3D surface model generated using the above-mentioned pipeline and a 3D ground truth model that was previously obtained through 3D laser scanning. Laser scanning was carried out using a high-precision laser scanner (Faro Focus 120), after which a surface model was manually generated. This allowed us to benchmark between the two models using several metrics including (a) the Euclidean distances between surface vertices, (b) the absolute difference between surface vertex coordinates, (c) the differences between six surface normals, and (d) the difference between room volumes (Figure 8). To calculate the first three metrics, we first align the two models by intersecting one vertex of each model (Vertex 5).

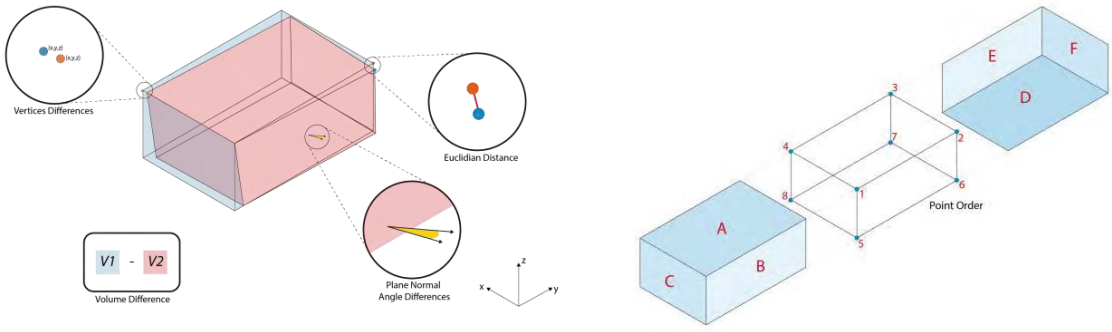

Figure 8. Comparison metrics, where the blue box represents the ground truth geometry and the red represents the generated geometry (left) and the principles of model alignment (right).

The results can be seen in Table 1. The difference between plane normals are calculated as 0.87, 1.06, 0.29, 0.56, 0.36 and 0.42 respectively for surfaces A to F. The precision of the results is within tolerable limits for energy modeling. Finally, the volumes of the two models are calculated as 170.78

and 156.14 m^3 for the ground truth and calculated geometries, which amount to a -8.5% difference. This error mostly stems from the scaling and pose adjustment steps. Since the points are selected by mouse clicks, selecting the exact points that correspond to the calculated 3D point correspondences remain a serious challenge against model precision. A feasible way of decreasing the error is the use of higher resolution images as input, which can enable more precise point selection.

Table 1. Euclidean and absolute differences between surface vertex coordinates of the two models

Vertex Id	Difference in x-dimension (m)	Difference in y-dimension (m)	Difference in z-dimension (m)	Euclidian Distance (m)
1	-0.02	-0.06	0.11	0.13
2	-0.33	-0.08	0.02	0.34
3	-0.30	-0.21	-0.04	0.37
4	-0.01	-0.23	0.06	0.24
5	0.00	0.00	0.00	0.00
6	-0.31	-0.02	-0.03	0.32
7	-0.28	-0.19	-0.08	0.35
8	0.01	-0.21	-0.05	0.22

3.2 Building energy modeling

In this section, we benchmark the energy simulation results of the energy model built using the proposed approach and using theoretical R-values. First, an EnergyPlus model of the classroom was built with OepnStudio, using the previously generated building surfaces. Following, two alternatives are considered for the R-values of the external wall. The first is the calculated value using the pipeline, and the second is the theoretical R-value associated with reinforced concrete material of the same thickness as the actual wall in the DesignBuilder material library. The other material thermal characteristics used in both models can be found in Table 2. The windows are modeled as double-glazed window (U= 2.6 W/m2-k, SHGC = 0.75, VT = 0.8). The internal load templates defined in DesignBuilder for people, lighting and equipment are used. The heating setpoint and setback temperatures are set to 22 C° (5:00AM-6:00PM during weekdays) and 18 C° respectively. Infiltration is set to 25ACH at 50Pa. The simulation run period was set to 24-30 December, which was the week that the actual measurements were taken. The variables in Equation 4 were measured as $T_{inside,air}$ = 23.1 C°, $T_{outside,air}$ = 1.0 C° and $T_{inside,reflected}$ = 27.0 C°. The U value was calculated as 2.0 W/m2-k, which is %40 lower that the theoretical value. However, it is consistent with a previous study that presents in-situ measurements of the same building wall using Infrared Thermography from the external environment by Sayin et al. (2016), who measured the U value as 2,07±0,38. According to the same study, this difference is possibly due to the use of high-quality concrete with a lower conductivity value than the standards.

Table 2. The thermal characteristics of the opaque materials in the energy models

Building Element	Material	Thickness (mm)	ALTERNATIVE 1: Theoretical U value (W/m2-k)	ALTERNATIVE 2: Calculated U value (W/m2-k)
Wall	Concrete, cast-dense, reinforced	250	**3.316**	**2.0**
Roof	Concrete, Reinforced	130	0.577	0.577
	Waterproofing membrane	-		
	XPS - CO2 blowing	50		
	Roofing felt	4		
	Stone chipping	10		
Floor	Ceramic floor tiles	20	2.840	2.840
	Cast Concrete, Dense	80		

The performance metrics are operative temperature, heating energy use and conductive heat loss through the external wall surfaces. We evaluate the percent change in these metrics from the theoretical to calculated R-valued models. The results indicate that the use of calculated R-values have varying degrees of influence (Table 3, Figure 9). The total heat loss through the envelope for the given week has decreased by 9.88%, due to the lower heat transfer rate through the surface. As a result, a decrease of 12.27% in the heating energy use was observed.

Table 3. The results of the energy simulations for the two models

	Total Heating (KW)	Total Heat Loss through Enve. (KW)	Total Heat Loss through walls (KW)	Average Oper. Temp (C)
Simulation with Theoretical U values	1132.50	1552.80	-454.40	18.33
Simulation with Calculated U values	993.50	1399.40	-264.90	18.49
% Change	12.27	9.88	41.70	0.83

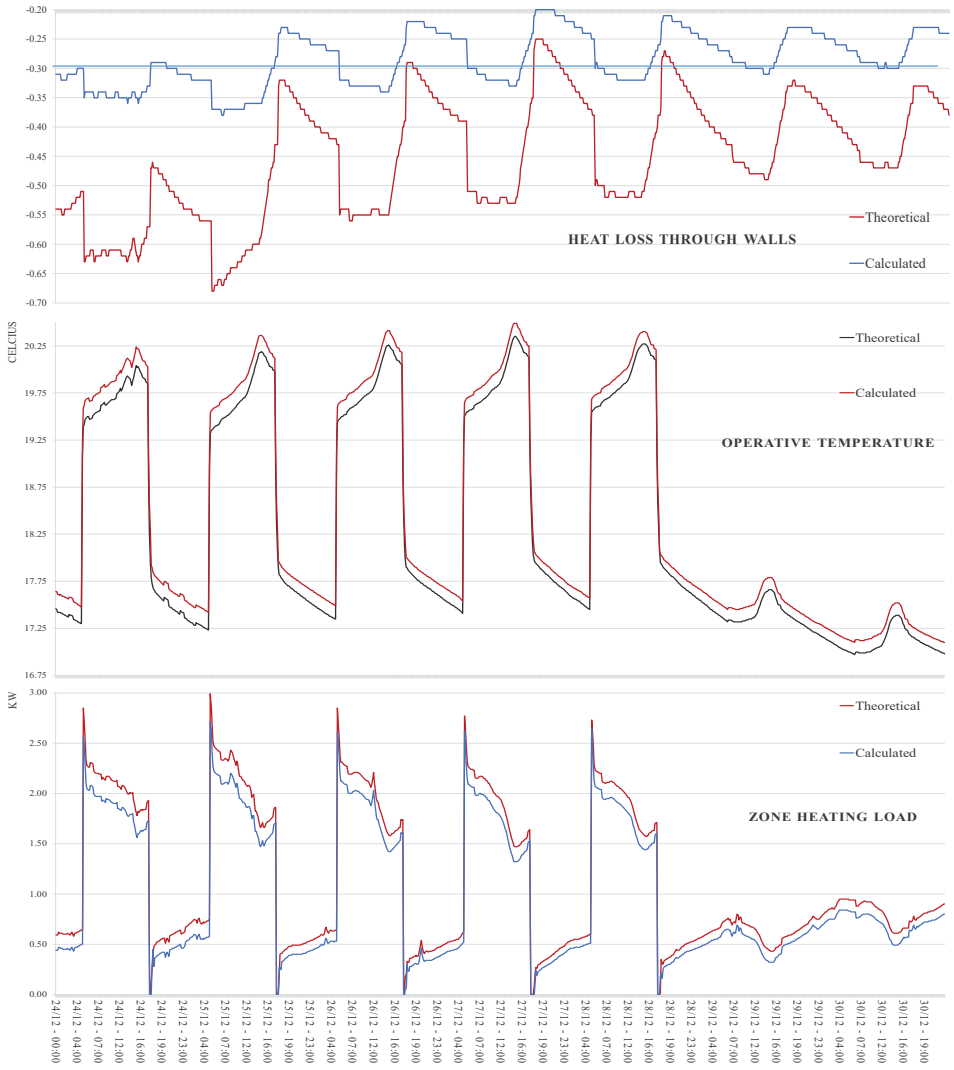

Figure 9. Evaluation metrics for building energy performance (24-30 December)

4. Conclusion

This paper proposed a pipeline for semi-automated energy modeling of existing buildings using 3D reconstruction. The pipeline was evaluated in a room, wherein the electrooptic images, thermal images and the environmental conditions (room and outside it temperature, reflected temperature) were first captured. Two comparative analyses were carried out to evaluate the precision of the 3D model and the level of impact of the newly calculated thermal transmittance value of the external wall on energy performance metrics. Although the building proportions and surface angles are within tolerable limits (<2), the calculated model scale is smaller than the actual dimensions. This is believed to be due to the imprecision in user's selection on digital images. The calculated U value, on the other hand, is %40 lower that the theoretical value of a wall with the same thickness and material. However, our results are consistent with a previous study conducted on the same building wall. The building energy simulations based on the energy models were evaluated through several building performance metrics. The results show that the calculated U-value of the external wall has a considerable influence on these metrics as compared to the theoretical U-value due to the reduced heat loss through the walls. The proposed pipeline is currently being implemented into a proof-of-concept software tool. In the future, tests will be made that involve the identification and registration of the windows and doors onto the walls, and the modeling of multiple adjacent rooms.

Acknowledgements

The authors would like to acknowledge the support by the TUBITAK-British Council's Newton – Katip Celebi Fund, Grant No. 217M519.

References

Akinci, B., Boukamp, F., Gordon, C., Huber, D., Lyons, C., & Park, K. (2006). A formalism for utilization of sensor systems and integrated project models for active construction quality control. *Automation in Construction*, *15*(2), 124–138. https://doi.org/https://doi.org/10.1016/j.autcon.2005.01.008

Bosché, F., & Guenet, E. (2014a). Automating surface flatness control using terrestrial laser scanning and building information models. *Automation in Construction*, *44*, 212–226. https://doi.org/https://doi.org/10.1016/j.autcon.2014.03.028

Bosché, F., & Guenet, E. (2014b). Automating surface flatness control using terrestrial laser scanning and building information models. *Automation in Construction*, *44*, 212–226. https://doi.org/10.1016/j.autcon.2014.03.028

Bosché, F., Guillemet, A., Turkan, Y., Haas, C., & Haas, R. (2013). Tracking the Built Status of MEP Works: Assessing the Value of a Scan-vs.-BIM System. *Journal of Computing in Civil Engineering*, *28*. https://doi.org/10.1061/(ASCE)CP.1943-5487.0000343

Cheng, J., Leng, C., Wu, J., Cui, H., & Lu, H. (2014). Fast and Accurate Image Matching with Cascade Hashing for 3D Reconstruction. In *2014 IEEE Conference on Computer Vision and Pattern Recognition* (pp. 1–8). https://doi.org/10.1109/CVPR.2014.8

Dimitrov, A., & Golparvar-Fard, M. (2014). Vision-based material recognition for automated monitoring of construction progress and generating building information modeling from unordered site image collections. *Advanced Engineering Informatics*, *28*(1), 37–49. https://doi.org/https://doi.org/10.1016/j.aei.2013.11.002

Furukawa, Y., & Ponce, J. (2010). Accurate, dense, and robust multiview stereopsis. IEEE transactions on pattern analysis and machine intelligence, 32(8), 1362-1376.

Ham, Y., & Golparvar-Fard, M. (2013). An automated vision-based method for rapid 3D energy performance modeling of existing buildings using thermal and digital imagery. *Advanced Engineering Informatics*, *27*(3), 395–409. https://doi.org/https://doi.org/10.1016/j.aei.2013.03.005

Hensen, J., & Lamberts, R. (2011). Introduction to building performance simulation. *Journal of Physics D-Applied Physics - J PHYS-D-APPL PHYS*.

Lowe, D. G. (2004). Distinctive Image Features from Scale-Invariant Keypoints. *International Journal of Computer Vision*, *60*(2), 91–110. https://doi.org/10.1023/B:VISI.0000029664.99615.94

M. A. Fischler, R. C. B. (1981). Random Sample Consensus: A Paradigm for Model Fitting with Applications to Image Analysis and Automated Cartography. *Communications of the ACM*, *24*, 381–395.

Mahdavi, A. (2001). Simulation-based control of building systems operation. *Building and Environment*, *36*(6), 789–796. https://doi.org/https://doi.org/10.1016/S0360-1323(00)00065-2

Mahdjoubi, L., Moobela, C., & Laing, R. (2013). Providing real-estate services through the integration of 3D laser scanning and building information modelling. *Computers in Industry*, *64*(9), 1272–1281. https://doi.org/https://doi.org/10.1016/j.compind.2013.09.003

Moulon, P., Monasse, P., & Marlet, R. (2012). Adaptive Structure from Motion with a contrario model estimation 1 Introduction 2 Structure from Motion the classical pipeline. *Lect. Notes Comput. Sci. (Including Subser. Lect. Notes Artif. Intell. Lect. Notes Bioinformatics)*, *7727 LNCS*(PART 4), 1–14. https://doi.org/10.1007/978-3-642-37447-0{_}20

Moulon, P., Monasse, P., Perrot, R., & Marlet, R. (2017). OpenMVG: Open Multiple View Geometry BT - Reproducible Research in Pattern Recognition. In B. Kerautret, M. Colom, & P. Monasse (Eds.) (pp. 60–74). Cham: Springer International Publishing.

Sayin, M., Tavukcuoglu, A. (2016). Cephelerin Isi Yalitimlilik Durumlarinin Isil Görüntüleme İle Değerlendirilmesi. Yalitim, Is Dunyasi Yayincilik, Istanbul.

Sweeney, C. (2015). Theia multiview geometry library: Tutorial & reference. University of California Santa Barbara.

Valero, E., Adan, A., & Cerrada, C. (2012). Automatic Method for Building Indoor Boundary Models from Dense Point Clouds Collected by Laser Scanners. *Sensors (Basel, Switzerland)*, *12*, 16099–16115. https://doi.org/10.3390/s121216099

Wang, S., Yan, C., & Xiao, F. (2012). Quantitative energy performance assessment methods for existing buildings. *Energy and Buildings*, *55*, 873–888. https://doi.org/https://doi.org/10.1016/j.enbuild.2012.08.037

Weaver, E., Long, N., Fleming, K., Schott, M., Benne, K., & Hale, E. (2019). Rapid Application Development with OpenStudio: Preprint.

Winkelmann, D. B. C. and C. O. P. and L. K. L. and F. C. (2000). EnergyPlus: Energy Simulation Program. *ASHRAE Journal*, *42*, 49–56.